Second order mode-finding method in dynamic stiffness matrix methods

Si Yuan[a], Kangsheng Ye[a], F.W. Williams[b],*

[a] *Department of Civil Engineering, Tsinghua University, Beijing 100084, China*
[b] *Department of Building and Construction, City University of Hong Kong, 83 Tat Chee Avenue, Kowloon, Hong Kong*

Received 21 May 2002; accepted 20 January 2003

Abstract

This paper addresses the transcendental eigenvalue problem, which arises for those structures, e.g., frames, for which dynamic member stiffnesses are available and are exact, in the sense that the appropriate differential equations have been solved. Thus it does *not* relate to traditional finite element vibration (or buckling) methods which are approximate and give a linear eigenvalue problem which can be solved by many excellent methods.

The well-established Wittrick–Williams algorithm is a powerful, reliable and efficient means of obtaining the desired number of natural frequencies for transcendental eigenvalue problems but, except for one very recent paper involving explicit derivatives and a recursive method, the corresponding vibration mode computations suffer from various difficulties and far from match the elegance of the frequency computations. This paper presents a newly developed, mathematically elegant and computationally efficient algorithm for accurate and reliable computation of vibration modes. It uses standard inverse iteration with approximate natural frequencies of only first order accuracy to produce the corresponding vibration modes to second order accuracy. Extrapolation can then be used to improve the original natural frequencies to second order accuracy. Moreover, the algorithm automatically provides a helpful so-called "$\tilde{\mu}$-check" which enables the acceptability of the mode accuracy to be judged. Numerical examples presented include some demanding ones, e.g., with coincident natural frequencies. These show the excellent performance of the method. Two advantages over the recent recursive paper are that explicit derivatives are replaced by differencing and recursion is avoided. In combination, these two advantages make the new method much more suitable for retrofitting into existing computer programs.
© 2003 Elsevier Ltd. All rights reserved.

*Corresponding author. Tel.: +852-2194-2045; fax: +852-2788-7612.
  E-mail address: bcfred@cityu.edu.hk (F.W. Williams).

1. Introduction

1.1. General introduction

This paper does not relate to traditional finite element vibration (or buckling) methods, which discretize a problem into approximately represented finite elements, the number of which depends upon the accuracy required, and which result in a linear eigenproblem for which many solution methods and a voluminous literature exist. Instead, it relates to those frames and other structures for which the differential equations of component members can be solved to obtain exact dynamic member stiffness matrices, so that exact results are obtained without the need to divide members into elements. Hence, the global dynamic stiffness matrix of the structure is a transcendental function of frequency, i.e., its elements are trigonometric and/or hyperbolic functions of frequency. There is relatively little literature on the solution of the resulting transcendental eigenproblem, which can be expressed as

$$\mathbf{K}(\omega)\mathbf{D} = \mathbf{0}. \tag{1}$$

Here $\mathbf{D}$ is the displacement amplitude vector for the joints at which the members are connected together and $\mathbf{K}(\omega)$ is the global dynamic stiffness matrix, each stiffness coefficient of which is a transcendental function of the frequency ω. Note that because these methods are "exact", there is no need to divide the members into parts by introducing joints, i.e., nodes, along their lengths except for the exceptional cases described later in this paper. Note also that the examples in this paper are for plane frames and are solved by using existing member dynamic stiffness matrices [1] without the need for further subdivision, as done in static stiffness matrix methods.

It is assumed that the natural frequencies to which the required modes correspond have already been obtained. Although exact natural frequencies are the ideal objective, they are usually found only to a certain number of digits or, exceptionally, to virtually machine accuracy. The most successful and reliable methods [1–4] for computation of natural frequencies in dynamic stiffness matrix methods all use the Wittrick–Williams (or W–W) algorithm [1,5–7] and so it is adopted in this paper as our work method.

To date, with one exception, mode-finding methods associated with the natural frequencies given by the W–W algorithm have been relatively crude, in the sense that they yield relatively low accuracy and insufficient robustness. The exception is a very recent and powerful recursive method [8], which obtains extremely accurate natural frequencies and modes whenever the cost of doing so is justified. It has many relationships with the method presented in the present paper which are indicated at appropriate places in this paper. The motivation for the present paper is that the recursive paper needs explicit expressions for the derivatives of the member stiffnesses which, coupled with its recursive nature, make it harder to implement in new computer programs and an order of magnitude harder to retrofit to the large body of existing programs than is the method presented in this paper. This is the motivation for the new method, which is extremely accurate and robust but, above all, relatively simple to implement.

1.2. Key features of the Wittrick–Williams algorithm

The W–W algorithm does not directly compute the natural frequencies. Instead, it gives the total number of natural frequencies below an arbitrarily chosen frequency $\omega = \omega^*$ as

$$J = J_0(\omega^*) + s\{\mathbf{K}(\omega^*)\}. \tag{2}$$

Here $s\{\mathbf{K}\}$ is the *sign count* of $\mathbf{K}$, which is calculated as the number of negative leading diagonal elements of the upper triangular matrix $\mathbf{K}^\Delta$ obtained from $\mathbf{K}$ by ordinary Gaussian elimination and; J_0 is the number of natural frequencies below ω^* when all the joint displacements $\mathbf{D}$ are constrained to be zero. For convenience, the natural frequencies of any member with both ends fixed are denoted by ω_F and are called member fixed-end frequencies, with the corresponding modes being called local ones. Hence $J_0 = \sum J_m$, where J_m is the number of ω_F of a member subject to $\omega_F < \omega^*$, and the summation is over all members. Repeated use of Eq. (2) yields several alternative iterative methods [1–4] which effectively narrowly bound the sought natural frequency ω_g within the *frequency interval*, (ω_l, ω_u), where ω_u and ω_l are upper and lower *frequency bounds*, i.e.,

$$\omega_u - \omega_l < Tol \times (1 + \omega_u). \tag{3}$$

Here *Tol* is the user specified error tolerance and Eq. (3) effectively combines the relative error control (good for magnitude of ω around unity) and absolute error controls (good for large and very large ω) to cover both ordinary order and small values of ω_g.

The simplest but slowest of the alternative iterative methods use bisection, as follows. If the ith natural frequency is required, at step 1 J is computed from Eq. (2) at a trial value of ω^*, which becomes an initial value of ω_u if $J \geqslant i$ and otherwise becomes an initial value of ω_l. An initial value of the opposite bound is then found by repeating step 1, with ω^* halved or doubled respectively, as many times as necessary. Then step 2 bisects to obtain $\omega^* = (\omega_u + \omega_l)/2$, uses Eq. (2) to calculate J and alters ω_u to $\omega_u = \omega^*$ if $J \geqslant i$ and otherwise alters ω_l to $\omega_l = \omega^*$. This step is repeated until Eq. (3) is satisfied.

An important corollary of the W–W algorithm, which is used extensively in this paper, is that the numbers of natural frequencies N_r and of member fixed-end frequencies N_{r0} in the frequency interval are

$$N_r = J|_{\omega_u} - J|_{\omega_l}, \quad N_{r0} = J_0|_{\omega_u} - J_0|_{\omega_l}. \tag{4a, b}$$

The N_r natural frequencies are multiple if $N_r > 1$ and are taken as $(\omega_l + \omega_u)/2$.

1.3. Classification of vibration modes

As a precursor to discussing earlier mode-finding methods for the transcendental eigenproblem, it is useful to first classify vibration modes into three physically distinct types. These are the global, local and mixed ones of Table 1, as is now explained in detail.

Global modes are defined as ones for which at least some of the joint displacements participate, i.e., $\mathbf{D} \neq \mathbf{0}$, and no member of the structure has a fixed-end frequency effectively coincident with the natural frequency of the structure, so that $N_{r0} = 0$. In this paper this coincidence is interpreted as $\omega_l < \omega_F < \omega_u$ and is indicated by $\omega_F \cong \omega_g$. (All modes are global ones for traditional finite element methods unless refinements such as exact substructuring are used.)

Table 1
Classification of vibration modes

Type	$\mathbf{D}$	N_{r0}	In frequency interval (ω_l, ω_u)	
			Any ω_F?	Any $K_{ij} \to \infty$?
Global	$\neq \mathbf{0}$	$= 0$	None	None
Local	$= \mathbf{0}$	> 0	Some	Some
Mixed	$\neq \mathbf{0}$	> 0	Some	Some

Local modes are defined as ones for which all joint displacements are nodal in the mode, i.e., $\mathbf{D} = \mathbf{0}$, so that inevitably $N_{r0} > 0$.

Mixed modes are defined as ones for which one or more members have $\omega_l < \omega_F < \omega_u$, but for which nevertheless some or all of the displacements of the joints participate, i.e., $\mathbf{D} \neq \mathbf{0}$ [9]. Hence again $N_{r0} > 0$.

Computationally, global modes are the easiest to handle because $N_{r0} = 0$. In contrast $\omega_F \cong \omega_g$ for the other two mode types, so that a trivial analysis of the member stiffness coefficients k_{rs} shows them to be infinite at ω_F, so that some coefficients K_{ij} of $\mathbf{K}(\omega^*)$ are also infinite. Hence the first, second and fourth columns of Table 1 define the three mode types while the remaining two columns contain consequences.

An alternative physically based argument for why $K_{ij} \to \infty$ when $\omega_F \cong \omega_u$ is that, because ω_F corresponds to a member vibrating without any end displacements, k_{rs} clearly becomes infinite because multiplying it by a zero displacement gives a finite end clamping force. This physical reasoning also suggests the use of a local "bubble shape" vibration mode, with amplitude C, whenever $\omega_F \cong \omega_g$. The alternative of using C directly is not adopted in this paper, in which instead it is in effect used implicitly by inserting an interior node which is positioned such that neither of the sub-members formed has $\omega_F \cong \omega_g$ [8]. This converts both local and mixed vibration modes into global ones and hence unifies the approach to the three different types of vibration mode.

Fig. 1 presents a simple example to illustrate global, local and mixed modes, plus the use of interior nodes. The frame has three identical, rigidly connected, horizontal or vertical inextensible members with their far ends built-in, see Fig. 1(a). The W–W algorithm of Eq. (2) shows that two natural frequencies coincide when $\omega = \omega_F$, i.e., $\omega_g = \omega_F$ and $N_r = 2$. However, an infinite set of possible pairs of independent modes exists because any one possible pair can be combined in any proportions to give further modes. Figs. 1(b)–(d) show three modes can be readily deduced because each involves two members vibrating with equal amplitudes and no end displacements, which ensures moment equilibrium at the sole joint of the frame. However, as expected, only two of them are independent, because (b) = (c) + (d).

Fig. 1(e) indicates the sole joint necessary, i.e., joint 1 of Fig. 1(a), and Figs. 1(f)–(h) introduce mid-length interior nodes into, respectively, the one, two or three members indicated by reference to Fig. 1(a). Arrows indicate the degrees of freedom at the nodes, so that, for Figs. 1(e)–(h), respectively, $\mathbf{D}$ contains 1, 3, 5 and 7 displacement amplitudes. The words at Fig. 1(i)–(t) categorize the mode types for the 12 alternative combinations of mode and joint positions.

The independence and orthogonality of the modes for coincident natural frequencies are now briefly discussed, to make the rest of the paper more readily intelligible. Any two of the three
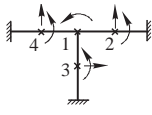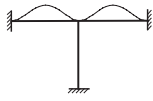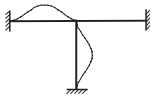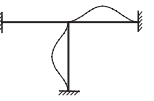
Joints present	Three possible modes		
(a)	(b)	(c)	(d)
(e) 1	(i) local	(j) local	(k) local
(f) 1,2	(l) mixed	(m) local	(n) mixed
(g) 1,2,3	(o) mixed	(p) mixed	(q) mixed
(h) 1,2,3,4	(r) global	(s) global	(t) global

Fig. 1. Illustrative frame example, used for three purposes: (1) the first row shows the frame and three possible modes for $\omega_g = \omega_F$; (2) the first column shows the joint freedoms before and after the introduction of one, two or three interior nodes and; (3) the remaining entries, i.e., (i)–(t), form a table which gives the type of mode for the joint/node positioning indicated in the first column and the mode, i.e., (b)–(d), given in the first row.

modes of Figs. 1(b)–(d) can be chosen as an independent pair. Unfortunately, none of these three possible pairs have the desirable feature of being mutually orthogonal. However, it is readily seen that mode (d) is orthogonal to the mode obtained by summing modes (b) and (c), because the members are identical and so the product of the (normalized) amplitudes for the three members are 0, $\frac{1}{2}$ and $-\frac{1}{2}$, which sum to zero.

1.4. Review of existing methods

Methods should accommodate all mode cases. Earlier methods, called (M1)–(M5) here, include [10]: (M1) when $N_r = 1$, solving $\mathbf{K}^\Delta \mathbf{D} = \mathbf{0}$ by giving the last element of $\mathbf{D}$ an arbitrary value; (M2) instead solving $\mathbf{K}^\Delta \mathbf{D} = \mathbf{0}$ with the last $h - 1$ elements of $\mathbf{D}$ null and the hth from last element having an arbitrary value, where h is the distance up the diagonal of $\mathbf{K}^\Delta$ to its lowest negative element when $\omega = \omega_u$; (M3) when $N_r > 1$, repeating (M2) for the N_r lowest negative elements of $\mathbf{K}^\Delta$ at $\omega = \omega_u$; (M4) when $N_r = 1$, solving $\mathbf{KD} = \mathbf{P}$ for a random $\mathbf{P}$ and; (M5) when $N_r > 1$, repeating (M4) for N_r different random $\mathbf{P}$'s.

Table 2(b) defines the criteria (C1)–(C11) used in Table 2(a) to indicate the performance of the older methods (M1)–(M5), of the recent recursive method [8], which is denoted by (M6), and (in anticipation) of the method presented in this paper. None of the older methods satisfy (C11), which includes the infinite number of displacements within members, but (M3) and (M5) can be made to do so by using an appropriate orthogonalization procedure [11]. Note that although (M1)–(M5) are old methods the small amount of more recent work on mode-finding methods (other than (M6)) essentially consists of refinements of (M1)–(M5) to produce mode-finding methods which complement the natural frequencies already obtained by the W–W algorithm. Hence, the contents of Table 2 establish the need for new mode-finding

Table 2
Comparison of methods: (a) assessment of the methods M1–M6 defined in the text and; (b) definitions of the criteria used in (a). Note that for C1–C5 an element of subjective judgement is used to score from 10 (Excellent) to 1, whereas criteria C6–C11 are either passed ($\sqrt{}$) or failed ($\times$)

(a)

Method	Criterion										
	C1	C2	C3	C4	C5	C6	C7	C8	C9	C10	C11
M1	9	9	9	8	3	$\times$	$\sqrt{}$	$\times$	$\times$	$\times$	$\times$
M2	8	9	9	8	4	$\sqrt{}$	$\sqrt{}$	$\times$	$\times$	$\times$	$\times$
M3	6	8	8	8	5	$\sqrt{}$	$\sqrt{}$	$\times$	$\times$	$\sqrt{}$	$\times$
M4	7	7	8	8	7	$\sqrt{}$	$\sqrt{}$	$\times$	$\times$	$\times$	$\times$
M5	6	6	6	6	6	$\sqrt{}$	$\sqrt{}$	$\times$	$\times$	$\sqrt{}$	$\times$
M6	3	10	7	10	10	$\sqrt{}$	$\sqrt{}$	$\sqrt{}$	$\sqrt{}$	$\sqrt{}$	$\sqrt{}$
present	7	8	8	9	9	$\sqrt{}$	$\sqrt{}$	$\sqrt{}$	$\sqrt{}$	$\sqrt{}$	$\sqrt{}$

(b)

Criterion		Description
Method is	C1	simple
	C2	fast
	C3	cheap
	C4	accurate
	C5	reliable
	C6	Useable when last element of $\mathbf{D}$ is zero
Method can find	C7	Global modes
	C8	Local modes
	C9	Mixed modes
	C10	N_r independent modes when $N_r > 1$
	C11	N_r orthogonal modes when $N_r > 1$

methods for the transcendental eigenvalue problem, such as (M6) and the new method presented in this paper.

2. The new high precision method

2.1. The basic theory

It is assumed temporarily that $\mathbf{K}'_g$ and $\mathbf{K}''_g$ are calculable and the following notation is used:

$$\omega_m = \frac{\omega_u + \omega_l}{2}, \quad \Delta\omega = \omega_u - \omega_l,$$

$$\mathbf{K}_l = \mathbf{K}(\omega_l), \quad \mathbf{K}_m = \mathbf{K}(\omega_m), \quad \mathbf{K}_u = \mathbf{K}(\omega_u),$$

$$\mathbf{K}_g = \mathbf{K}(\omega_g), \quad \mathbf{K}'_g = \frac{\mathrm{d}\mathbf{K}(\omega_g)}{\mathrm{d}\omega}, \quad \mathbf{K}''_g = \frac{\mathrm{d}^2\mathbf{K}(\omega_g)}{\mathrm{d}\omega^2}. \tag{5}$$

The cases in which $\mathbf{K}'_g$ and $\mathbf{K}''_g$ are incalculable clearly correspond to one or more members having $\omega_F \cong \omega_g$. Therefore, they can be overcome by inserting an interior node into any such member [8], so that neither sub-member thus created has $\omega_F \cong \omega_g$, and then defining $\mathbf{K}$ to be the stiffness matrix after insertion of all such nodes. The appropriate positioning of these interior nodes is covered in the next section.

Initially, consider the single root case, i.e., the W–W algorithm has shown that there is exactly one natural frequency ω_g in (ω_l, ω_u), so that $N_r = 1$. Suppose also that $\omega_m = \frac{1}{2}(\omega_l + \omega_u)$ is taken as the approximate natural frequency. When $\omega \equiv \omega_g$, $\det(\mathbf{K})(= \det(\mathbf{K}_g)) = 0$ and the exact mode vector $\mathbf{D}_g$ is the solution of $\mathbf{K}_g \mathbf{D}_g = \mathbf{0}$. However, at ω_m the matrix product of $\mathbf{K}_m$ and $\mathbf{D}_g$ will not vanish, i.e., $\mathbf{K}_m \mathbf{D}_g \neq \mathbf{0}$. Then a Taylor series expansion with respect to the natural frequency ω_g leads to

$$\mathbf{K}_m \mathbf{D}_g = \mathbf{K}_g \mathbf{D}_g + (\omega_m - \omega_g)\mathbf{K}'_g \mathbf{D}_g + \frac{(\omega_m - \omega_g)^2}{2} \mathbf{K}''_g \mathbf{D}_g + O((\Delta\omega)^3). \tag{6}$$

In the recent recursive method [8], it was assumed that explicit expressions are available for the derivatives of the member stiffnesses k_{rs} and hence for $\mathbf{K}'$. Therefore, it was not necessary for ω_l and ω_u to be close together and so widely separated bounds were used to obtain the first result, which was then improved recursively. However, for many types of member such explicit expressions are not available, e.g., for most non-uniform ones, and so here $\mathbf{K}'_g$ is replaced by the difference expression (7). Then noticing that $\mathbf{K}_g \mathbf{D}_g = \mathbf{0}$ and $\omega_u - 2\omega_g + \omega_l = 2(\omega_m - \omega_g)$ enables Eq. (6) to be written as Eq. (8)

$$\mathbf{K}'_g = \frac{\mathbf{K}_u - \mathbf{K}_l}{\omega_u - \omega_l} - \frac{(\omega_u - 2\omega_g + \omega_l)}{2} \mathbf{K}''_g + O((\Delta\omega)^2), \tag{7}$$

$$\mathbf{K}_m \mathbf{D}_g = \frac{\omega_m - \omega_g}{\omega_u - \omega_l}(\mathbf{K}_u - \mathbf{K}_l)\mathbf{D}_g - \frac{(\omega_m - \omega_g)^2}{2} \mathbf{K}''_g \mathbf{D}_g + O((\Delta\omega)^3). \tag{8}$$

Working to first order only gives the standard generalized eigenproblem

$$\mathbf{K}_m \mathbf{D} = \tilde{\mu}(\mathbf{K}_u - \mathbf{K}_l)\mathbf{D}, \tag{9}$$

where $\mathbf{D}$ approximates $\mathbf{D}_g$ very closely. (Note that $\tilde{\mu}$ is used here to avoid confusion with the slightly different μ of the recent recursive method [8]).

Comparing Eqs. (8) and (9) gives

$$\tilde{\mu} \cong \frac{\omega_m - \omega_g}{\omega_u - \omega_l}. \tag{10}$$

Hence for the range used below, i.e., $\omega_l < \omega < \omega_u$, to a very good approximation

$$|\tilde{\mu}| < \tfrac{1}{2}. \tag{11}$$

Eqs. (9) and (11) are the governing equations for finding $\mathbf{D}$, i.e., for finding $\mathbf{D}_g$ to high accuracy (for higher accuracy closer bounds ω_u and ω_l can be used, unless their closeness causes ill-conditioning). Eqs. (9)–(11) are very instructive and lead naturally to an algorithm with several attractive and desirable features, as follows.

2.2. Inverse iteration

Solving Eq. (9) involves many eigenpairs but, because $N_r = 1$, only one of them satisfies $\omega_l < \omega < \omega_u$. Hence, only the numerically smallest eigenvalue $\tilde{\mu}$ can satisfy Eq. (11). A method that is guaranteed [12] to converge on the eigenpair giving this eigenvalue is the inverse iteration procedure

$$
\left.
\begin{aligned}
\bar{\mathbf{D}}^{(k+1)} &= \mathbf{K}_m^{-1}(\mathbf{K}_u - \mathbf{K}_l)\mathbf{D}^{(k)} \quad \text{with} \quad \mathbf{D}^{(0)} = \text{random vector,} \\
\tilde{\mu}^{(k+1)} &= \frac{1}{\bar{D}_i^{(k+1)}} \quad \text{with} \quad |\bar{D}_i^{(k+1)}| = \max_j |\bar{D}_j^{(k+1)}|, \\
\mathbf{D}^{(k+1)} &= \tilde{\mu}^{(k+1)}\bar{\mathbf{D}}^{(k+1)},
\end{aligned}
\right\} \quad k = 0, 1, \ldots,
$$

(12a)

which is terminated when

$$
\max_i \left| D_i^{(k+1)} - D_i^{(k)} \right| < Tol1 \quad \text{or} \quad k = k_{\max},
$$

(12b)

where $D_i^{(k)}$ is the ith element of $\mathbf{D}^{(k)}$, $Tol1$ is the user specified error tolerance which may not be equal to Tol in Eq. (3), and $k_{\max}$ is the specified maximum number of iterations allowed. Note that since $\mathbf{D}^{(k)}$ has been normalized previously, only absolute error control is used in Eq. (12b). This is the basic method used for computation of mode vectors in this paper and it gives excellent approximations, ω (see Eq. (22) below) and $\mathbf{D}$, to ω_g and $\mathbf{D}_g$. (Note that to ensure convergence to the absolutely smallest eigenpair, the initial mode vector $\mathbf{D}^{(0)}$ is composed of random numbers in the range of (0,1).)

3. Position of interior nodes

When inserting an interior node into a member of length L which has an $\omega_F \cong \omega_g$, its position must be chosen such that the sub-members produced have neither $\omega_F \cong \omega_g$ nor such unequal lengths that numerical instability may occur. The earlier paper [8] gives a general method for locating interior nodes which can be applied to members regardless of their complexity, but admitted that it lacked the elegance of formulas where such can be obtained. Therefore, this section presents such formulas for Bernoulli–Euler beams with uncoupled axial behaviour, with proofs of their validity. For simplicity, the proofs are for $\omega_F = \omega_g$, because extension to $\omega_F \cong \omega_g$ is clearly possible.

Rule 1. *If $\omega = \omega_F$ and ω_F is a lateral member fixed-end vibration frequency, it is recommended that sub-members of length $L^* = L/2$ should be adopted when Bernoulli–Euler theory is used in the absence of axial loading.*

Proof. The global natural frequency ω_g satisfies the local characteristic equation [1]

$$
1 - \cosh \lambda \cos \lambda = 0 \quad \text{with} \quad \lambda = L\left(\sqrt[4]{\frac{m\omega_g^2}{EI}}\right),
$$

(13)

where m is the mass per unit length and EI the flexural rigidity. If the global natural frequency ω_g coincides with any sub-member ω_F, it must simultaneously satisfy

$$
1 - \cosh(\lambda^*) \cos(\lambda^*) = 0 \quad \text{with} \quad \lambda^* = \lambda/2.
$$

(14a)

Since $\cosh(\lambda^*) > 0$, this can be written as

$$\cos(\lambda^*) = \frac{1}{\cosh(\lambda^*)}, \tag{14b}$$

while Eq. (13) can be written as

$$1 - (2\cosh^2\lambda^* - 1)(2\cos^2\lambda^* - 1) = 0. \tag{15}$$

Substituting Eq. (14b) into Eq. (15) shows that Eqs. (14b) and (15) hold true simultaneously only if

$$2(\cosh\lambda^* - \cos\lambda^*)^2 = 0. \tag{16}$$

This requires $\lambda^* = 0$, which represents an irrelevant rigid body mode. Hence, Eqs. (13) and (14a) cannot hold simultaneously, which completes the required proof that sub-members with $L^* = L/2$ cannot have a flexural ω_F coincident with ω_g. $\square$

Rule 2. *If $\omega = \omega_F$ and ω_F is a fixed-end axial vibration frequency of a member, it is recommended that sub-members of lengths*

$$L^{(1)} = \left(\frac{1}{2} - \frac{1}{2k}\right)L \quad and \quad L^{(2)} = \left(\frac{1}{2} + \frac{1}{2k}\right)L, \quad k = 2, 4, 6, \ldots, \tag{17a}$$

$$L^{(1)} = L^{(2)} = \frac{L}{2}, \quad k = 1, 3, 5, \ldots \tag{17b}$$

should be used where

$$k = \frac{v}{\pi} \quad with \quad v = \omega_g L\sqrt{\frac{m}{EA}} \tag{18}$$

and EA is the extensional rigidity of the member.

Proof. The global natural frequency ω_g satisfies the local characteristic equation $\sin v = 0$ [1], which gives $v = k\pi$, $(k = 1, 2, 3, \ldots)$. Calculating $v^{(i)}$ from $L^{(i)}$ $(i=1,2)$ for $v = k\pi$ gives

$$v^{(1)} = \frac{k}{2}\pi - \frac{\pi}{2}, \quad v^{(2)} = \frac{k}{2}\pi + \frac{\pi}{2}, \quad k = 2, 4, 6, \ldots,$$

$$v^{(1)} = v^{(2)} = \frac{k}{2}\pi, \quad k = 1, 3, 5, \ldots$$

and inserting the above into the local characteristic equation gives

$$\left|\sin v^{(i)}\right| = 1, \tag{19}$$

i.e., $\sin v^{(i)} \neq 0$ and so the global natural frequency ω_g is no longer a fixed-end frequency ω_F for either sub-member. $\square$

Note that Rule 1 prevents a member with a flexural $\omega_F \cong \omega_g$ from being replaced by sub-members with their flexural $\omega_F \cong \omega_g$, but their value of v must also be examined if it closely approximates $k\pi$, an *axial* $\omega_F \cong \omega_g$. Similarly, Rule 2 must be supplemented by checking that $1 - \cosh \lambda^{(i)} \cos \lambda^{(i)}$ $(i = 1, 2)$ is not dangerously close to zero.

4. Advantages of the new method

Of course, $\mathbf{K}_m$ is not inverted but instead is factored once only into $\mathbf{LAL}^T$, where $\mathbf{A}$ is a diagonal matrix, because each iteration step requires only forward- and back-substitution. Additionally, since the right-hand side vector $\mathbf{D}^{(k)}$ is known at each iteration step, the right-hand product vector can be calculated coefficient by coefficient so that $\mathbf{K}_u$ and $\mathbf{K}_l$ need not be formed and stored. Finally, as when using the W–W algorithm to converge on the natural frequency, pivoting is rarely found to be necessary, so that the symmetric, banded and sparse properties of $\mathbf{K}$ can be fully utilized.

While the frequency error is $|\omega_m - \omega_g|$, Eqs. (8) and (9) provide strong evidence that the mode vector error is second order, i.e., of order $(\omega_m - \omega_g)^2$ and this, plus all the numerical evidence available to them, has convinced the authors that this method is second order even though no strict proof is given. Such accuracy means that ω_m need not approximate ω_g very closely, e.g., if machine accuracy is 14 decimal digits, computed mode vectors will achieve almost machine accuracy for any ω_m satisfying $|\omega_m - \omega_g| < 10^{-7}$, i.e., the user can specify $Tol \cong 10^{-7}$ in Eq. (3). This reduces the chances of ill-conditioning compared with Ref. [8].

Because the error is dominated by $(\omega_m - \omega_g)^2$ and is unaffected by (ω_l, ω_u), slightly enlarging the interval (ω_l, ω_u) while keeping ω_m unaltered is an optional means of improving the conditioning and hence the accuracy of the difference approximation (7) to $\mathbf{K}'_g$. However, such tuning appears not usually to be necessary.

Because $\mathbf{K}(\omega)$ is a dynamic stiffness matrix in this paper it is never linear in ω^2 $(= \lambda$ say). However it would be for a typical finite element free vibration problem because then the problem degenerates to $\mathbf{KD} = \lambda \mathbf{MD}$, for which the proposed algorithm gives an exact formulation, as follows:

$$\mathbf{K}_m = \mathbf{K} - \lambda_m \mathbf{M}, \quad \mathbf{K}_u - \mathbf{K}_l = -(\lambda_u - \lambda_l)\mathbf{M}. \tag{20}$$

Hence Eq. (8) reduces to

$$(\mathbf{K} - \lambda_m \mathbf{M})\mathbf{D} = (\lambda - \lambda_m)\mathbf{MD} \tag{21}$$

and cancelling the $\lambda_m \mathbf{MD}$ terms returns Eq. (21) to the original form $\mathbf{KD} = \lambda \mathbf{MD}$.

The first order natural frequency accuracy does not match the second order mode vector accuracy. However, whenever the computed $\tilde{\mu}$ satisfies Eq. (11), extrapolation Eq. (10) gives the second order accuracy approximation

$$\omega_\mu = \omega_m - \tilde{\mu}(\omega_u - \omega_l). \tag{22}$$

One of the most desirable features of the proposed formulation is the $\tilde{\mu}$-*check* of Eq. (11), i.e., $|\tilde{\mu}| < \frac{1}{2}$. Although not a necessary condition for an approximate solution, it gives a valuable indication of the quality of the solution, as follows. If $\tilde{\mu}$ from Eq. (9) satisfies Eq. (11) then the

corresponding mode vector $\mathbf{D}$ is reasonably acceptable and Eq. (22) can be used to obtain the better natural frequency ω_μ. Otherwise, if the $\tilde{\mu}$-check fails, the solution requires further improvement not because of insufficient accuracy, but due to it being unreliable because the extrapolated frequency ω_μ given by Eq. (22) lies outside the range (ω_l, ω_u) for which it is known that $N_{r0} = 0$. In practice, the results in this paper and all others obtained by the authors confirm the expectation that inverse iteration for narrow ranges (ω_l, ω_u) is unlikely to cause failure of the $\tilde{\mu}$-check and even less likely to cause erroneous results. Nevertheless, whenever it occurs the computations should ideally be repeated for a different value of *Tol* in order to alter ω_l and ω_u.

The second order accuracy of the mode vector and of ω_μ allows larger error tolerances *Tol* to be used ($\cong$ to the square root of the desired tolerance) for the iterative convergence on the natural frequency that precedes the mode computations. Hence, it requires fewer iterations. This considerably reduces the total time needed to find a natural frequency and its associated mode, because it is dominated by these iterations and by the approximately equally time consuming factorization of $\mathbf{K}_m$ in Eq. (12a).

The inverse iteration applied to the eigenproblem of Eq. (9) is essentially an accelerated version due to root shifting and so converges very rapidly, especially when $\omega_m \cong \omega_g$. This is easily seen by assuming that the interval (ω_l, ω_u) is very small and recalling that the convergence rate of the inverse iteration for the *i*th eigenpair is characterized by the ratio of the *i*th and $(i+1)$th eigenvalues ($|\tilde{\mu}_i| < |\tilde{\mu}_{i+1}|$), i.e.,

$$\rho = \left|\frac{\tilde{\mu}_i}{\tilde{\mu}_{i+1}}\right| \cong \left|\frac{\omega_{g,i} - \omega_m}{\omega_{g,i+1} - \omega_m}\right| << \left|\frac{\omega_{g,i}}{\omega_{g,i+1}}\right|. \tag{23}$$

5. Multiple natural frequencies

Suppose that the W–W algorithm shows that $N_r > 1$ in (ω_l, ω_u). Then, if (ω_l, ω_u) is small enough, Eq. (9) will give exactly N_r eigenvalues that satisfy Eq. (11). These may be completely coincident or merely very close together, but in either case they are found as the first N_r numerically smallest eigenvalues of Eq. (9). Because this is a pure linear algebraic eigenproblem the N_r required eigenpairs can be obtained one by one by using the inverse iteration procedure of Eq. (12a) with the usual orthogonalization procedure. For example, if the first $i - 1(<N_r)$ eigenpairs have been obtained the *i*th eigenpair can be computed by setting the initial vector to

$$\tilde{\mathbf{D}}_i^{(0)} = \mathbf{D}_i^{(0)} - \sum_{j=1}^{i-1} \alpha_j \mathbf{D}_j. \tag{24}$$

Here $\mathbf{D}_i^{(0)}$ is a random vector, $\mathbf{D}_j$ is the *j*th eigenvector of those already obtained, and orthogonalization gives α_j as

$$\alpha_j = \frac{\mathbf{D}_j^{\mathrm{T}}(\mathbf{K}_u - \mathbf{K}_l)\mathbf{D}_i^{(0)}}{\mathbf{D}_j^{\mathrm{T}}(\mathbf{K}_u - \mathbf{K}_l)\mathbf{D}_j}. \tag{25}$$

Because $\tilde{\mathbf{D}}_i^{(0)}$ is orthogonal to the first $i - 1$ eigenvectors the iteration cannot converge to any previously obtained eigenvector. Additionally, coincident natural frequencies are distinguished

from very close ones by comparing the computed eigenvalues $\tilde{\mu}$ and the extrapolated frequencies ω_μ. However, if the N_r eigenvalues are very close rather than being identical, the convergence rate ρ approaches unity and so the inverse iteration could converge very slowly. To help to rectify this, the well-known simultaneous or subspace iteration method, e.g., see Chapter 10 of Ref. [12], has been adopted in this paper, although brevity requires omission of its details. (Note that for coincident natural frequencies the convergence may no longer be second order.)

6. Illustrative examples

For simplicity, units are ignored in the following numerical examples. In the first two examples, the mode vectors were found for all natural frequencies lying between given frequency bounds and *Tol* and *Tol*1 were not specified, so that the inverse iteration continued until the exact answer was converged on. For the remaining examples, error tolerances *Tol* and *Tol*1 were given and the frequency bounds were determined by using the W–W algorithm. The examples were chosen carefully to test and reflect the overall performance of the mode computations and are ordered such that simple, easy and small problems precede more complex, difficult and larger ones. Throughout, about 14 decimal digits were used for floating point number calculations and the Fortran 90 computer code used was run on a standard Pentium Pro 200 MHz PC.

The examples are mainly based on those of the earlier recursive paper [8]. They are needed because the present method converges to its final solution in a completely different way because it is not recursive and uses differencing in place of explicit expressions for the derivatives.

6.1. Example 1

This example is axial vibration of the rod shown in Fig. 2 with $m = EA = L = 1$, where m is the mass per unit length and EA the extensional rigidity. Its exact natural frequencies are

$$\omega_g = \tfrac{1}{6}\pi, \ \ \tfrac{1}{2}\pi, \ \ \tfrac{5}{6}\pi, \ \ \tfrac{7}{6}\pi, \ \ \tfrac{3}{2}\pi, \ \ \tfrac{11}{6}\pi, \ \ \ldots .$$

The two member mesh used was chosen deliberately to make $\omega_g = \pi/2, \ 3\pi/2, \ \ldots$ identical to the ω_F of the second member, so that interior nodes needed to be inserted when the modes corresponding to those frequencies were calculated.

Solution: Rule 2 shows that for both cases a central node is the recommended choice. The modes corresponding to the typical examples of $\omega_g = \pi/6$ and $\omega_g = 3\pi/2$ were computed, with a central node inserted into the second member for the $3\pi/2$ case.

The frequency bounds ω_l and ω_u assigned both approximated ω_g to only about two decimal places. Table 3 shows the computed results ω for the natural frequencies $\omega_g = \pi/6$ and $3\pi/2$ and shows that convergence to the exact solutions $\mathbf{D}_g$ (normalized to make the first component unity)
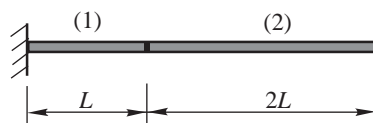

Fig. 2. Vibration of a rod (Example 1)

Table 3
Numerical results for **D** at each iteration for Example 1

ω_g	$\pi/6$	$3\pi/2$
ω_m	0.53	4.71
ω_l	0.52	4.70
ω_u	0.54	4.72
0	{1,1}	{1,1,1}
1	{1,2.00386864017409}	{1,0.008002532834336, −0.988757409703173}
2	{1,1.99999004813192}	{1,0.000013890216254, −0.999967349535445}
3	{1,2.00000002563382}	{1,0.000000044952386, −0.999999950230350}
…	…	…
6	{1,2.00000000000000}	{1,0.000000000000000, −1.000000000000000}
Exact	{1,2}	{1,0,−1}

took six iterations. The extrapolated natural frequencies ω_μ and their relative errors (to 3 significant figures) were then, respectively,

$$\omega_\mu = 0.523653496861917, \ 4.71239010403247,$$

$$\left|\frac{\omega_\mu - \omega_g}{\omega_g}\right| = 1.05 \times 10^{-4}, \ 2.38 \times 10^{-7}. \tag{26}$$

The errors in ω_μ are clearly roughly the square of the relative errors in ω_m, which are 1.22×10^{-2} for $\omega_g = \pi/6$ and 5.07×10^{-4} for $\omega_g = 3\pi/2$, i.e., the extrapolated natural frequencies have second order accuracy.

6.2. Example 2

This example is vibration of the cross-shaped rigidly jointed frame shown in Fig. 3, which has four identical members. (The modes and joints 2–5 shown on Fig. 3 are not required for this example but are needed by Example 3). The members have $m = EI = L = 1$, but with their extensional rigidity $EA = 10^4$ to give them sensible slenderness ratios. Its first three natural frequencies are $\omega_{g1} = 15.418206$ and $\omega_{g2} = \omega_{g3} = 22.274740$, i.e., the second and third natural frequencies are coincident. The corresponding mode vectors, i.e., $\{u_1, v_1, \theta_1\}$ at the centre joint, were computed.

Solution: For the first natural frequency, an initial vector $\{1, 1, 1\}$ was assumed with $\omega_l = 15.4$, $\omega_m = 15.5$ and $\omega_u = 15.6$. After three inverse iterations the mode vector was $\mathbf{D}^{(3)} = \{0.0000000000 \ \ 0.0000000000 \ 1\}$, which is exact to within 10 decimal places. The extrapolated frequency and its relative error were, respectively,

$$\omega_\mu = 15.41918308, \ \left|\frac{\omega_\mu - \omega_g}{\omega_g}\right| = 6.34 \times 10^{-5}. \tag{27}$$
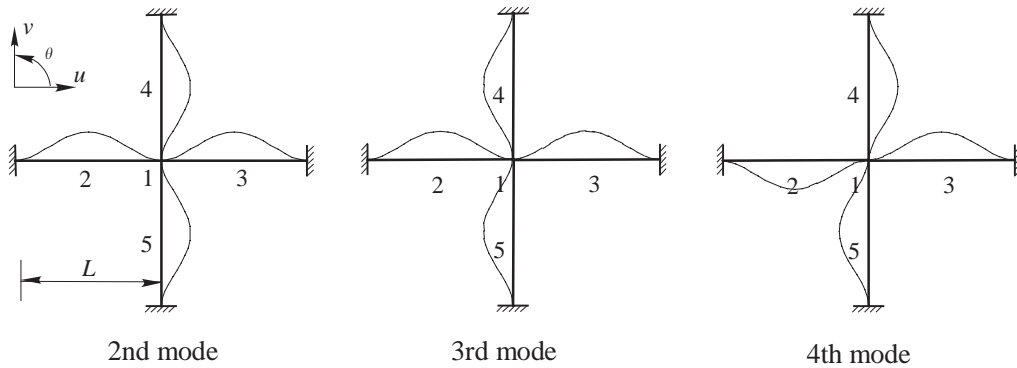
Fig. 3. Cross-shaped rigidly jointed frame and its mode shapes for ω_{g2}, ω_{g3}, and ω_{g4} (Examples 2 and 3).

For the second and third frequencies an initial vector $\{1,1,1\}$ was assumed with $\omega_l = 22.26$, $\omega_m = 22.27$ and $\omega_u = 22.28$. After eight inverse iterations the mode vector obtained was

$$\mathbf{D}^{(8)} = \{1 \ 1 \ 0.0000000000\}, \tag{28}$$

which is again exact to within 10 decimal places. Subsequent iterations with an initial vector orthogonal to the above one easily led to $\mathbf{D} = \{1 \ -1 \ 0.0000000000\}$, which is clearly orthogonal to the $\mathbf{D}^{(8)}$ of Eq. (28), by analogy with the earlier discussion of Fig. 1. The extrapolated frequency and its error were, respectively,

$$\omega_\mu = 22.274720, \quad \left|\frac{\omega_\mu - \omega_g}{\omega_g}\right| = 8.98 \times 10^{-7}. \tag{29}$$

It is informative to give an example where the $\tilde{\mu}$-check is not passed due to extremely wide and biased initial bounds. Such an example is to find the fifth frequency $\omega_{g5} = 49.96486$ with bounds $\omega_l = 40$, $\omega_u = 50$. The results after three inverse iterations were $\tilde{\mu} = -0.6017691$, $\omega_\mu = 51.01769$ and the error changed as follows:

$$\left|\frac{\omega_m - \omega_g}{\omega_g}\right| = 9.94 \times 10^{-2}, \quad \left|\frac{\omega_\mu - \omega_g}{\omega_g}\right| = 2.11 \times 10^{-2}.$$

As expected, second order accuracy was not achieved because the $\tilde{\mu}$-check failed. Nevertheless, the accuracy order was improved by obtaining ω_μ instead of using ω_m and hence the results were still reasonably acceptable. There is also a hint that the upper bound $\omega_u = 50$ is very likely to be a better choice for the extrapolated ω_μ.

Taking three bisection steps aided by the W–W algorithm leads to the alternative cases $\omega_l = 45$, 47.5 or 48.75, with $\omega_u = 50$ unchanged. The $\tilde{\mu}$-check failed for the first two cases and for $\omega_l = 48.75$ the results were

$$\tilde{\mu} = -0.4915181, \quad \omega_\mu = 49.98939$$

and the errors were

$$\left|\frac{\omega_m - \omega_g}{\omega_g}\right| = 1.18 \times 10^{-2}, \quad \left|\frac{\omega_\mu - \omega_g}{\omega_g}\right| = 4.91 \times 10^{-4}.$$

Here although the $\tilde{u}$-check was still only just passed, a much better order of accuracy was obtained and the most important fact is that the extrapolated frequency was assured to be better than any of ω_l, ω_m or ω_u. To reach a frequency of at least the same accuracy as $\omega_u = 49.98939$ by bisection would require four more bisections.

6.3. Example 3

This example is again identical to Example 2 except that the axial rigidity was increased to $EA = 10^6$ to crudely approximate inextensible members. Its first four natural frequencies are $\omega_{g1} = 15.418206$, $\omega_{g2} = \omega_{g3} = 22.372319$ and $\omega_{g4} = 22.373285$, so that the coincident second and third ones are very close to the fourth one, which is also the lowest fixed-end frequency ω_F of all four members and corresponds to a local mode with $\mathbf{D} = \mathbf{0}$.

Solution: This might be expected to complicate the mode computations. Instead of assigning frequency bounds ω_l and ω_u, error tolerances Tol and $Tol1$ were given to control the solution accuracy for both frequencies and mode vectors. Two cases were considered, namely $Tol = 0.5 \times 10^{-3}$ and $Tol = 0.5 \times 10^{-4}$, with $Tol1 = Tol^2$ to give mode vectors to second order accuracy. Members were not initially given interior nodes and so $\mathbf{D}$ consisted of the three displacements $\{u_1, v_1, \theta_1\}$ at the central joint 1 in Fig. 3. Interior nodes were inserted at the centres of the members when necessary to give $\mathbf{D}^*$ and were numbered as shown in Fig. 3. Tables 4 and 5, in which $\mathbf{D}^* = \{u_1, v_1, \theta_1, u_2, v_2, \ldots, \theta_5\}$, give the computed results and Fig. 3 shows the mode shapes.

Using $Tol = 0.5 \times 10^{-3}$ caused all three clustered frequencies ω_2, ω_3 and ω_4 to lie between ω_l and ω_u and hence to appear coincident. As predicted by the preceding theory, the extrapolation technique within the mode computation algorithm increased the frequency accuracy tremendously and also separated ω_4 from the truly coincident ω_2 and ω_3, while the computed mode vectors are as exact as $Tol1 = 0.25 \times 10^{-6}$ allowed.

The higher frequency specified by $Tol = 0.5 \times 10^{-4}$ resulted in the three clustered frequencies ω_2, ω_3 and ω_4 being separated into two intervals, one containing ω_2 and ω_3 and the other ω_4. The

Table 4
Computed results for ω_2, ω_3 and ω_4 of Example 3

Tol	0.5×10^{-3}	0.5×10^{-4}
(ω_l, ω_u)	$(22.364377, 22.373413)^a$	$(22.371465, 22.372595)^b$, $(22.372868, 22.373687)^c$
$\Delta\omega = \omega_u - \omega_l$	0.009036^a	0.001130^b
		0.000819^c
$\omega_{2m} = \omega_{3m}$ (Err)	22.368895^a (0.003424)	22.372030 (0.000289)
ω_{4m} (Err)	(0.004390)	22.373277 (0.000008)
$\omega_{2\mu} = \omega_{3\mu}$ (Err)	22.372319 (0)	22.372329 (0.000010)
$\omega_{4\mu}$ (Err)	22.373286 (0.000001)	22.373285 (0)
Number of subspace iterations	3	10
		4
Expanded $\mathbf{K}^*$ used?	For all three frequencies	Only for ω_4

Notes: Err $= \omega_m - \omega_g$ or $\omega_\mu - \omega_g$.
[a] For ω_2, ω_3 and ω_4.
[b] For ω_2 and ω_3.
[c] For ω_4.

Table 5
Computed mode vectors corresponding to ω_2 and ω_4 for Example 3

$Tol = 0.5 \times 10^{-3}$		$Tol = 0.5 \times 10^{-4}$	
D* for ω_2	**D*** for ω_4	**D*** for ω_2	**D*** for ω_4
1.3096423E−4	−3.8992294E−17		1.5671659E−12
1.2692544E−4	−1.0771324E−17		1.1363897E−12
9.6579140E−14	6.3896244E−9		1.4078678E−24
6.5486210E−5	−1.9510510E−17		7.8363198E−13
0.96916118	−1.0000000		−1.0000000
2.4260579E−4	−1.7500798E−9		2.1720997E−12
6.5486210E−5	−1.9510532E−17	1.0000000	7.8363198E−13
0.96916118	1.0000000	0.44867910	1.0000000
−2.4260579E−4	−1.7497613E−9	−1.2690872E−29	−2.1720997E−12
1.0000000	1.0000000		1.0000000
6.3466693E−5	−5.3911215E−18		5.6823040E−13
2.5032553E−4	−1.7502208E−9		2.9954870E−12
1.0000000	−1.0000000		−1.0000000
6.3466693E−5	−5.3910716E−18		5.6823040E−13
−2.5032553E−4	−1.7492648E−9		−2.9954870E−12

frequency accuracy was again greatly increased by the extrapolation technique. When using subspace iteration to find ω_2 and ω_3 and their modes, $\omega_3(=\omega_2)$ was very close to the adjacent natural frequency $\omega_{g4}(\omega_{g3}/\omega_{g4} = 0.99996)$. So Eq. (23) gives $\rho \cong (\omega_{3\mu}-\omega_{3m})/(\omega_{4\mu}-\omega_{3m}) \cong 0.238$, which is far enough from unity to give fairly rapid convergence, which is why no more than 10 iterations were needed to satisfy $Tol1$. The convergence rate could have been greatly increased by applying the commonly used convergence improvement technique of using one or two extra vectors in the subspace iteration.

Note that in the $Tol = 0.5 \times 10^{-4}$ case, ω_2, ω_3 and their modes were found satisfactorily without inserting interior nodes even though this resulted in a pole at ω_{g4}, which is very close to ω_u because $\omega_{g4}-\omega_u = 0.00069$. As expected, this only moderately reduced the convergence rate and hence moderately increased the number of iteration steps.

Table 5 shows the mode shapes numerically because the graphical alternative lacks the precision needed by the above discussions. The first, fifth and higher modes were also computed without difficulty but are omitted for brevity.

6.4. Example 4

This example is an unbraced rigidly jointed one bay, 10 storey frame. All 30 members (i.e., 10 beams and 20 columns) are identical and almost inextensible, with $m = EI = L = 1$ and $EA = 10^6$.

Table 6
Fundamental mode: sways of beams for Example 4

Tol	10^{-3}	10^{-5}	10^{-11}
ω_{1m}	0.263<u>68713</u>	0.264035<u>820961</u>	0.26403937032<u>7</u>
$\omega_{1\mu}$	0.26403<u>960</u>	0.264039370<u>350</u>	0.264039370326
10	1.00000000	1.00000000	1.00000000
9	0.98029996	0.98029996	0.98029996
8	0.9372304<u>4</u>	0.93723043	0.93723043
7	0.8701114<u>7</u>	0.87011145	0.87011145
6	0.7804582<u>8</u>	0.78045825	0.78045825
5	0.6705705<u>7</u>	0.67057052	0.67057052
4	0.5433084<u>7</u>	0.54330842	0.54330842
3	0.4020672<u>0</u>	0.40206715	0.40206715
2	0.2512464<u>2</u>	0.25124638	0.25124638
1	0.1005735<u>0</u>	0.10057348	0.10057348

Notes: The left-hand column indicates storey level of beam. Underlined numbers are inaccurate digits. The number of inverse iterations was always 3.

Solution: Table 6 gives the storey beam sways of the fundamental mode calculated using three alternative tolerances *Tol*, with *Tol*1 = *Tol*. Since no exact solution is available, the *Tol* = 10^{-11} results were used to evaluate the accuracy of the natural frequencies and modes given by *Tol* = 10^{-3} and 10^{-5}. Clearly both the extrapolated natural frequencies and mode vectors are accurate to second order because the errors are better than Tol^2, even though *Tol*1 = Tol^2 was not specified.

6.5. Example 5

This example is identical to Example 4 except that *Tol*1 = Tol^2 and the unbraced frame was expanded to have 20 storeys and 10 bays.

Solution: The modes obtained cannot be tabulated for reasons of space, but again the extrapolated natural frequencies and mode vectors for *Tol* = 10^{-3} and 10^{-5} were accurate to second order.

However, this example was principally used to explore the speed of the method compared to existing methods for a medium-sized problem (**K** is 660×660). Such comparisons should ideally be obtained by running equally efficiently coded versions of the methods on the same computer. Even then the percentage time savings achieved by the method presented would not be the same for different structures, different required accuracy or different computers. Therefore the authors used their extensive experience of the earlier methods and their results from the method presented to estimate the time saving when obtaining results to engineering accuracy, taken to mean relative errors of approximately 10^{-4} for the natural frequencies and modes, i.e., $Tol \cong 10^{-2}$. Hence the method presented was estimated to save approximately 37% of the time needed by the random force vector method [13] when used with the fastest available method [2] for converging on a natural frequency prior to calculating the corresponding mode.

7. Conclusions

The new second order high precision method presented was carefully designed to meet all 11 of the criteria used in Table 2. Of these, the first five criteria (simplicity, speed, cost, accuracy and reliability) are all fundamentally desirable and were the major goals achieved, as described in the next five paragraphs.

Simplicity has been achieved by converting the non-linear (transcendental) eigenproblem mode computations into finding the fundamental eigenpair for a generalized linear matrix eigenproblem, i.e., Eq. (9). This is solved efficiently by inverse iteration or subspace iteration for, respectively, single and multiple fundamental eigenvalues. Therefore, the method is basically as simple as inverse or subspace iteration, i.e., as the commonest methods used for linear matrix eigenproblems.

High speed is achieved for three reasons. Firstly, only the fundamental eigenpair (single or multiple) is needed and this is usually the easiest one to obtain. Secondly, the inverse iteration for solving Eq. (9) is accelerated by automatically incorporating the root shift technique, see Eq. (23), to tremendously improve the convergence rate such that usually two to three iterations suffice. Thirdly, the second order accuracy of both the mode vectors and the extrapolated natural frequencies implies that the initial frequency bounds for the required mode and the natural frequency accuracy need be much less accurate, thus reducing the total computation time, e.g., by about a third when obtaining engineering accuracy for quite large structures, see Example 5.

Cheapness is achieved partly because of this reduced computation time. Reductions of memory required also contribute, as follows. The banding, sparseness and symmetry of the stiffness matrix can be used during ordinary Gauss elimination, thus sharing these advantages of the usual finite element methods. Additionally, the right-hand side product vector can be calculated coefficient by coefficient to avoid forming and storing the global matrices $\mathbf{K}_u$ and $\mathbf{K}_l$, thus optionally reducing the memory requirement by making a sacrifice of run time, which is usually moderate because normally very few inverse iterations are needed.

High accuracy is a major advantage, mainly because first order frequency bounds yield second order accuracy for both modes and the extrapolated natural frequencies. Hence, many of the numerical results presented appear to be exact to the full eight or more digits given. The second order accuracy also incidentally implies that the proposed method is exact for linear matrix eigenproblems, as opposed to for the transcendental eigenproblems of this paper.

High reliability is achieved from four sources. Firstly, the method correctly produces all required mode vectors, not just global ones. Secondly, all modes computed are automatically orthogonal even if they are multiple modes corresponding to coincident natural frequencies. Thirdly, the extrapolation of natural frequencies is able to separate any close natural frequencies, which appear to be coincident at the end of the initial natural frequency bounding calculations. Fourthly, the $\tilde{u}$-check automatically provides a useful means to assess any possible inaccuracy due to ill conditioning.

Appendix A. Nomenclature

D	global joint displacement amplitude vector
EA	extensional rigidity
EI	flexural (i.e., bending) rigidity
J	number of natural frequencies below ω^*
J_0	value of J if **D** is clamped, so that $\mathbf{D} = \mathbf{0}$
K	global dynamic stiffness matrix
$\mathbf{K}^\Delta$	upper triangular matrix obtained from **K** by standard Gauss elimination
L	length of member or element
m	mass per unit length of member
N_r	number of natural frequencies of structure in interval (ω_l, ω_u)
N_{r0}	number of ω_F in interval (ω_l, ω_u)
Tol	user specified error tolerance for frequency bounds
$Tol1$	user specified error tolerance for mode vectors
λ	dimensionless parameter for member flexure, see Eq. (13), or ω^2
$\tilde{\mu}$	eigenvalue of inverse iteration method
v	dimensionless parameter for member axial behaviour, see Eq. (18)
ρ	approximate convergence rate of inverse iteration
ω	frequency (rad/s)
ω^*	arbitrary value of ω

Subscripts

F	element fixed-end natural frequencies are ω_F
g	values at any exact natural frequency of structure
l	values at lower bound on ω_g
u	values at upper bound on ω_g
m	values half way between ω_l and ω_u
μ	second order approximation to ω_g, see Eq. (22)

References

[1] F.W. Williams, W.H. Wittrick, An automatic computational procedure for calculating natural frequencies of skeletal structures, International Journal of Mechanical Sciences 12 (9) (1970) 781–791.

[2] F.W. Williams, D. Kennedy, Reliable use of determinants to solve non-linear structural eigenvalue problems efficiently, International Journal for Numerical Methods in Engineering 26 (8) (1988) 1825–1841.

[3] D. Kennedy, F.W. Williams, More efficient use of determinants to solve transcendental structural eigenvalue problems reliably, Computers and Structures 41 (5) (1991) 973–979.

[4] J. Ye, F.W. Williams, A successive bounding method to find the exact eigenvalues of transcendental stiffness matrix formulations, International Journal for Numerical Methods in Engineering 38 (6) (1995) 1057–1067.

[5] F.W. Williams, W.H. Wittrick, Exact buckling and frequency calculations surveyed, Journal of Structural Engineering, American Society of Civil Engineers 109 (1) (1983) 169–187.

[6] W.H. Wittrick, F.W. Williams, A general algorithm for computing natural frequencies of elastic structures, Quarterly Journal of Mechanics and Applied Mathematics 24 (3) (1971) 263–284.

[7] A.Y.T. Leung, Dynamic Stiffness and Substructures, Springer, London, 1993.

[8] S. Yuan, K. Ye, F.W. Williams, D. Kennedy, Recursive second order convergence method for natural frequencies and modes when using dynamic stiffness matrices, International Journal for Numerical Methods in Engineering 56 (12) (2003) 1795–1814.

[9] F.W. Williams, S. Yuan, K. Ye, D. Kennedy, M.S. Djoudi, Towards deep and simple understanding of the transcendental eigenproblem of structural vibrations, Journal of Sound and Vibration 256 (4) (2002) 681–693.

[10] C.T. Hopper, F.W. Williams, Mode finding in nonlinear structural eigenvalue calculations, Journal of Structural Mechanics 5 (3) (1977) 255–278.

[11] K.L. Chan, F.W. Williams, Orthogonality of modes of structures when using the exact transcendental stiffness matrix method, Shock and Vibration 7 (1) (2000) 23–28.

[12] A. Jennings, Matrix Computation for Engineers and Scientists, Wiley, London, 1977.

[13] H.R. Ronagh, R. Lawther, F.W. Williams, Calculation of eigenvectors with uniform accuracy, Journal of Engineering Mechanics, American Society of Civil Engineers 121 (9) (1995) 948–955.